Original Article

The analysis and validation of the prediction value of conventional and contrast-enhanced ultrasonography for *BRAF* mutant papillary thyroid microcarcinoma

Huilin Li[1,2]^, Jiaojiao Ma[2], Xuehua Xi[2], Jiajia Tang[1,2], Linping Wang[1,2], Liangkai Wang[2,3], Shengtao Lin[4], Bo Zhang[1,2]^

[1]Chinese Academy of Medical Sciences and Graduate School of Peking Union Medical College, Beijing, China; [2]Department of Ultrasound, China-Japan Friendship Hospital, Beijing, China; [3]China-Japan Friendship Institute of Clinical Medicine, Beijing, China; [4]Bracco Imaging Medical Technologies Co., Ltd., Beijing, China

Contributions: (I) Conception and design: H Li, Lp Wang, J Ma, B Zhang; (II) Administrative support: B Zhang, S Lin; (III) Provision of study materials or patients: B Zhang; (IV) Collection and assembly of data: H Li, X Xi, J Tang, Lp Wang, Lk Wang; (V) Data analysis and interpretation: H Li, X Xi, J Tang, Lp Wang, Lk Wang; (VI) Manuscript writing: All authors; (VII) Final approval of manuscript: All authors.

Correspondence to: Bo Zhang. China-Japan Friendship Hospital, Beijing 100029, China. Email: thyroidus@163.com.

Background: *BRAF* has certain potential in distinguishing aggressive papillary thyroid microcarcinoma (PTMC). However, it is not recommended to conduct *BRAF* analysis for all suspicious thyroid nodules <1 cm. In order to investigate the ultrasound value indicating BRAF mutation among PTMC, which showed discrepancy in previous studies, we aimed to establish a predictive model based on conventional and contrast-enhanced ultrasonography.

Methods: We consecutively and retrospectively enrolled patients with PTMC who underwent fine-needle aspiration biopsy (FNAB) at our hospital between January 2020 and January 2021. All PTMC patients received conventional and contrast-enhanced ultrasound prior to FNAB, samples gained went through cytological analysis and BRAF testing subsequently. The following conventional ultrasonography data were analyzed: maximum diameter, echogenicity, echo homogeneity, echogenic foci, location, shape, boundary, aspect ratio, and blood flow volume. Moreover, the following contrast-enhanced ultrasonography data were also analyzed: degree, homogeneity, completeness, and enhancement method. Time-intensity curves from contrast-enhanced ultrasonography were analyzed using VueBox software for different regions of interest, including the entire tumor, the area of strongest enhancement, and healthy thyroid glands. The independent risk factors for *BRAF* mutation in PTMC were identified using univariate and multivariate logistic regression. Their predictive value was tested through internal validation.

Results: Of the 103 PTMC lesions analyzed, 72 involved *BRAF* mutations. Five independent ultrasonographic risk factors for *BRAF* mutation were identified: relative time to peak value in the area of strongest enhancement, unclear boundary, location adjacent to thyroid capsules, maximum diameter >0.5 cm, and punctate echogenic foci. A predictive model based on these factors was able to diagnose *BRAF* mutations in PTMC, with an area under the curve (AUC) of 0.824. During internal validation, this model showed an AUC of 0.723.

Conclusions: Conventional and contrast-enhanced ultrasound characteristics, including relative time to peak value in the area of strongest enhancement, unclear boundary, location adjacent to thyroid capsules, maximum diameter >0.5 cm, and punctate echogenic foci, may be useful for predicting *BRAF* mutations in patients with PTMC.

Keywords: *BRAF*; papillary thyroid microcarcinoma (PTMC); contrast-enhanced ultrasound; VueBox

^ ORCID: Huilin Li, 0000-0001-8053-7980; Bo Zhang, 0000-0003-3389-5018.

Submitted Aug 18, 2022. Accepted for publication Oct 10, 2022.
doi: 10.21037/gs-22-493
View this article at: https://dx.doi.org/10.21037/gs-22-493

Introduction

Thyroid cancer is one of the most common endocrine malignancies, with an incidence rate that has been increasing by approximately 20% annually worldwide (1) and cases in the United States (US) tripling in recent decades (2). Approximately 80–90% of thyroid cancer cases are papillary thyroid carcinoma (PTC) (3), and nearly 50% of PTCs involve tumors with a maximum diameter of no larger than 1.0 cm, which is known as papillary thyroid microcarcinoma (PTMC) (4).

The standard method for diagnosing thyroid cancer is fine-needle aspiration biopsy (FNAB) (5,6) along with simultaneous genetic testing for $BRAF^{V600E}$ (termed *BRAF* in the paper) mutation. The *BRAF* gene, with a Val600Glu substitution in the protein, encodes the most active of three RAF kinases and is the most frequent genetic mutation in thyroid cancer (7). It can predict PTCs with a positive predictive value of >99% (8).

FNAB is invasive, and technically difficult for potential PTMCs, especially for those smaller than 0.5 cm, or those close to trachea or recurrent laryngeal nerve. The American Thyroid Association recommends it only for suspicious thyroid nodules ≥1 cm, but *BRAF* mutation is associated with a higher risk of PTMC recurrence (7,9,10), which in turn strongly increases the risk of PTMC-related mortality and worsens prognosis (11-13). Since *BRAF* testing was always conducted using residual specimens through FNAB, we sought to explore a safer, non-invasive method to help predict PTMC involving *BRAF* mutation.

Previous studies have confirmed ultrasound features in evaluating the malignancy in thyroid nodules, some suggested that certain ultrasound findings correlate with *BRAF* mutation in PTCs, including the aspect ratio, microcalcification, nodule size after enhancement, as well as the enhancement method and time (14); centripetal and non-significant enhancement (15); or microbubble arrival time or time-to-peak (TTP) in quantitative contrast-enhanced ultrasonography (16). On the other hand, other studies have found no significant associations between ultrasound findings and *BRAF* mutation (17,18). However, most of these studies were based on objective ultrasonic findings and did not specify differences of PTMC among PTC cases.

Herein, we aimed to screen for ultrasound findings that may predict *BRAF* mutation in patients with PTMC. We explored the independent risk factors for such mutations using a combination of conventional and contrast-enhanced ultrasonography. We present the following article in accordance with the STARD reporting checklist (available at https://gs.amegroups.com/article/view/10.21037/gs-22-493/rc).

Methods

Patients

The study was conducted in accordance with the Declaration of Helsinki (as revised in 2013). This retrospective study was approved by institutional ethics board of China-Japan Friendship Hospital (No. 2019-103-K71). Individual consent for this retrospective analysis was waived. From January 2020 and January 2021, we consecutively enrolled 156 PTC patients underwent conventional and contrast-enhanced ultrasound with pathological results and potentially available for quantitative analysis. Eventually, we involved 103 PTMC patients, each with a single lesion, who (I) underwent fine needle aspiration biopsy between January 2020 and January 2021 at our hospital; (II) had cytologically or pathologically confirmed PTMC; (III) were older than 18 years; (IV) had available *BRAF* genotyping results; (V) were in Bethesda stage V or VI based on cytopathology or Bethesda stage I–IV and positive for *BRAF* mutation; (VI) had available contrast-enhanced ultrasound images in Digital Imaging and Communication in Medicine (DICOM) format adequate for quantitative analysis during >60 sec, in which sufficient healthy thyroid tissue adjacent to the tumor was visible to serve as a reference region of interest (ROI) (*Figure 1*).

Patients were excluded if they underwent total thyroidectomy, or if their ultrasound images showed a quality of fit (QOF) <30% after motion compensation. Patients were classified either as having mutant *BRAF* (*BRAF*-positive group) or as having wild-type *BRAF* (*BRAF*-negative group).

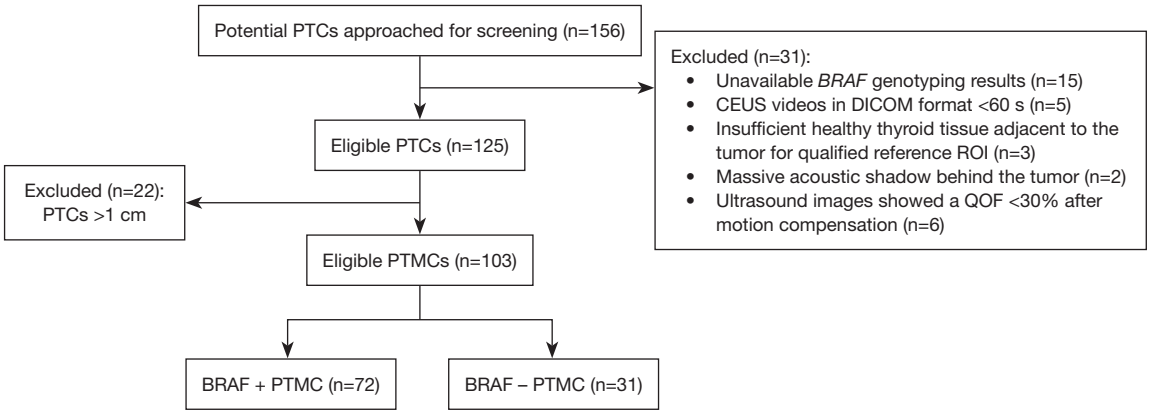

Figure 1 Flow diagram of 103 patients with papillary thyroid microcarcinoma stratified by *BRAF* genotype. PTCs, papillary thyroid carcinomas; CEUS, contrast-enhanced ultrasound; DICOM, Digital Imaging and Communication in Medicine; ROI, region of interest; QOF, quality of fit; PTMC, papillary thyroid microcarcinoma.

Conventional ultrasonography

Conventional ultrasonography was performed by radiologists with 5–20 years of experience in thyroid ultrasonography using a 5–14 MHz transducer (Siemens, ACUSON Sequoia, Siemens Medical Solutions USA, Inc.). The ultrasound contrast agent was sulphur hexafluoride microbubbles (SonoVue®, Bracco, Milan, Italy). Images were stored digitally as DICOM cine loops in the axial and/or sagittal planes of the thyroid nodules. Data on the following conventional ultrasound features were recorded: echogenicity, categorized as hyperechoic, isoechoic, hypoechoic, or very hypoechoic; echo homogeneity, homogeneous or heterogeneous; echogenic foci: none, punctate echogenic foci, macrocalcifications, or peripheral (rim) calcifications; location, distal from capsules or adjacent to them; margin, regular or irregular; boundary, unclear or clear; aspect ratio, ≤1 or >1; Adler blood flow volume (19), 0 (no blood flow signal in the tumor), 1 (1–2 punctate or short-stick blood flow signals in the tumor), 2 (3–4 punctate blood flow signals or one vessel with a clear wall in the tumor), or 3 (multiple colored blood flow signals in the tumor, with reticular or patchy distribution, or two vessels with clear walls).

Contrast-enhanced ultrasonography

Contrast-enhanced ultrasonography was performed using the same system and contrast agent as that for conventional ultrasonography. Following the detection of thyroid nodules, 0.5–2.4 mL of microbubble contrast agent was injected as an intravenous bolus, and contrast harmonic imaging was conducted at a reduced mechanical index of 0.09.

Data on the following contrast-enhanced ultrasound features were recorded: *degree of enhancement*, non-, hypo-, iso-, or hyper-enhancement; pattern of enhancement, centripetal or non-centripetal (the latter could be centrifugal or diffuse enhancement); homogeneity of enhancement, inhomogeneous or homogeneous; and completeness of enhancement, incomplete or complete.

Contrast-enhanced ultrasound images were further analyzed quantitatively using VueBox software (Bracco, Suisse SA, Geneva, Switzerland). We linearized DICOM cine loops, applied curve-fitting models, then evaluated time-intensity curves for the following parameters (*Figure 2*) (20): peak enhancement (arbitrary units, AU), defined as the maximum intensity of the curve; wash-in area under the curve (WiAUC, AU); wash-out area under the curve (WoAUC, AU); wash-in and wash-out areas under the curve (WiWoAUC, AU); wash-in rate (WiR), in terms of maximum slope (AU) (6); wash-out rate (WoR), in terms of minimum slope (AU); rise time (s); fall time (s); mean transit time local (mTTl, s); time-to-peak (TTP, s); wash-in perfusion index (WiPI), defined as WiAUC/rise time; and quality of fit (%) between echo-power signal and f (t). Data for these variables were plotted as parametric images (color-coded maps), to which time-intensity curves were fitted and linearized (*Figure 3*).

Furthermore, these variables were measured in various manually delineated ROIs. ROI 1 delineated the entire tumor boundary on conventional ultrasound images with reference to the corresponding contrast-enhanced image.

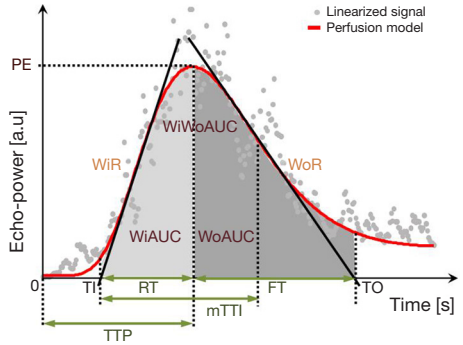

Figure 2 Time-intensity curve analysis of contrast-enhanced ultrasound features, based on ROI, as recommended by VueBox software. (Image reproduced with permission from VueBox documentation, seen online at https://www.contrastultrasound-modality.com/quantification-software/support/user-manual). WiAUC, wash-in area under the curve; mTTl, mean transit time local; TTP, time-to-peak; WiR, wash-in rate; WoR, wash-out rate; WoAUC, wash-out area under the curve; WiWoAUC, wash-in and wash-out areas under the curve; RT, rise time; FT, fall time; PE, peak enhancement; ROI, regions of interest; TI, the time at which the maximum slope tangent intersects the X-axis; TO, the time at which the minimum slope tangent intersects the X-axis.

ROI 2 was a 1-mm circle enclosing the area of greatest enhancement, which was identified based on color-coded imaging and peak enhancement values generated by VueBox. ROI 3 encircled a large normal thyroid gland without obvious vessels and surrounding the tumor in the same image acquisition plane and at the same depth as the tumor (*Figures 4,5*). The relative rise time and relative TTP for the whole tumor were defined as the ratios of the values in ROI 1 to the values in the reference ROI 3.

Analysis was performed in dual-screen mode for B-mode and contrast-enhanced ultrasonography, starting with the synchronization of B-mode and contrast-enhanced imaging of the first arterial loop. Contrast-enhanced ultrasound features were assessed using color-coded imaging in VueBox. The largest value of peak enhancement was colored dark red and the lowest value was colored dark blue. Also, the lowest values of rise time and TTP were colored dark red and the largest values were colored dark blue.

These variables above were assessed independently; if ambiguity was encountered, a more experienced radiologist made a decision.

Fine needle aspiration biopsy

Ultrasound-guided biopsy was performed by a radiologist with more than 20 years of experience in fine needle aspiration of thyroid nodules. Each suspected nodule was biopsied without suction using the freehand technique (15). At least two aspirations were performed in different directions. Samples obtained with 23-gauge needles were expelled onto glass slides, smeared, and immediately placed in 95% ethyl alcohol for Papanicolaou staining. Material left in the needle after aspiration was then used for molecular testing; DNA was extracted using the QIAGEN QIAamp DNA FFPE Tissue Kit (56404, QIAGEN) according to the manufacturer's protocol. The DNA spectral absorbance was measured by a spectrophotometer (SMA4000, Merinton, Beijing, China), and the DNA was diluted to approximately 2–3 ng/μL with an ATE (Tris Acetate-EDTA) elution buffer (QIAGEN).

The DNA was analyzed for the presence of *BRAF* mutation using a validated, China Food and Drug Administration (CFDA)-approved (State medical permitment number: No. 2010-3401226) Human *BRAF* ARMS-PCR (The tetra-primer amplification refractory mutation system-polymerase chain reaction) Kit (Amoy Diagnostics, Xiamen, China) based on the Amplification Refractory Mutation System (ARMS), with a forward primer of 5'-TCATAATGCTTGCTCTGATAGGA-3' and reverse primer of 5'-GGCCAAAAATTTAATCAGTGGA-3'. For each sample, there was an external control assay and a mutation assay (in the same well), and each run contained a negative and positive control. Thermal cycling was conducted on a Prism 7500 real-time PCR instrument (Life Technologies, Carlsbad, CA, USA) as follows: stage I, 5 min at 95 ℃; stage 2, 15 cycles of 25 s at 95 ℃, 20 s at 64 ℃, 20 s at 72 ℃; and stage 3, 31 cycles of 25 s at 93 ℃, 35 s at 60 ℃, 20 s at 72 ℃. Data were collected at 60 ℃ in stage 3.

Statistical analysis

The normality of data was tested using the Shapiro-Wilk test if no more than 50 data points were available, or using the Kolmogorov-Smirnov test if >50 data points were available. Homogeneity of variance was assessed using Levene's test. The inter-group differences in quantitative parameters were assessed for significance using an independent-samples *t*-test and Wilcoxon rank-sum test.

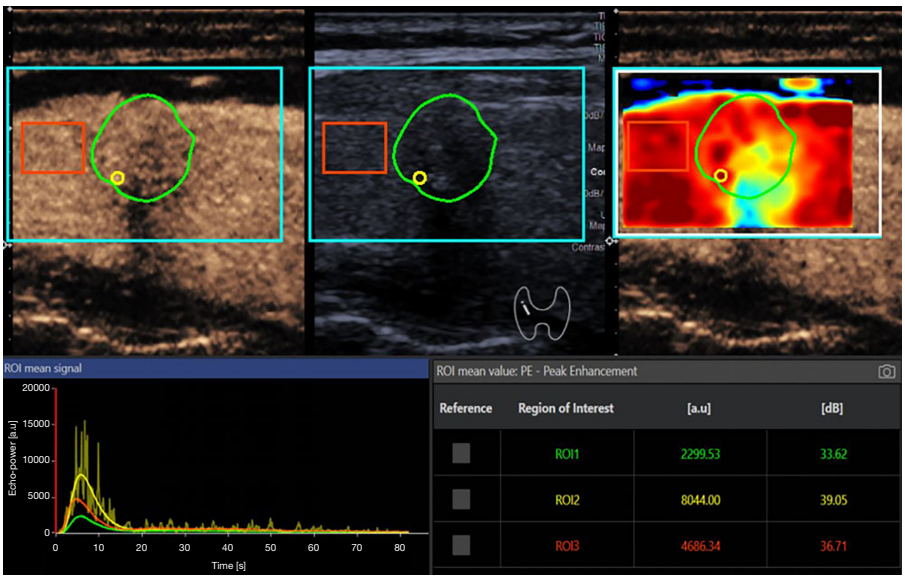

Figure 3 Example of a ROI-driven workflow for analyzing contrast-enhanced ultrasound images. Delimitation ROI (blue) delineates the processing area, excluding any non-echo data such as text, color bars, or image borders. ROI 1 (green) included the entire tumor boundary on conventional ultrasound with reference to the contrast-enhanced image. ROI 2 (yellow) included 1mm circles that targeted the greatest enhancement point, aided by the color-coded imaging and peak enhancement values generated by VueBox. ROI 3 (red) encircled a large surrounding normal gland including the same image acquisition plane in the same depth and without obvious vessels. Time-intensity curves were generated, and the color-coded perfusion parameters were analyzed. ROI, regions of interest.

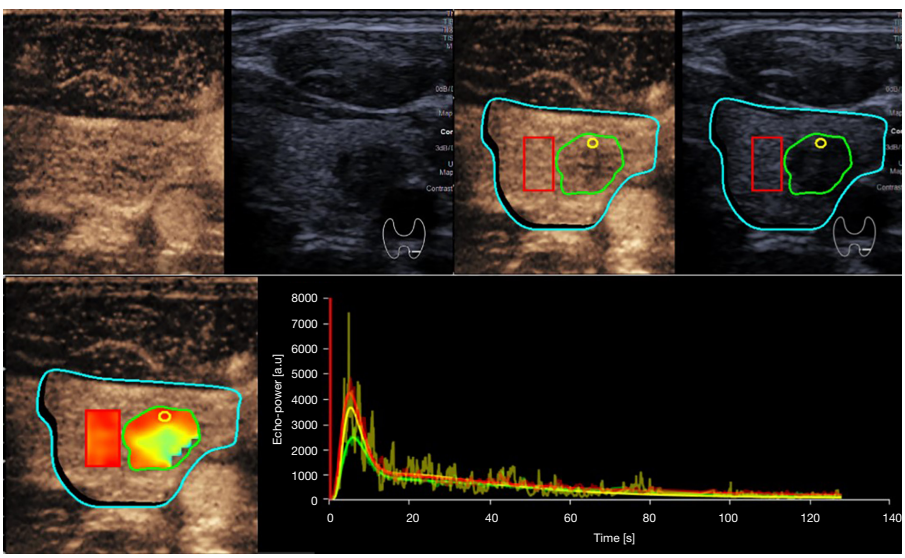

Figure 4 Example of ultrasound analysis. Delimitation ROI (blue) delineates the processing area, excluding any non-echo data such as text, color bars, or image borders. ROI 1 (green) included the entire tumor boundary on conventional ultrasound with reference to the contrast-enhanced image. ROI 2 (yellow) included 1mm circles that targeted the greatest enhancement point, aided by the color-coded imaging and peak enhancement values generated by VueBox. ROI 3 (red) encircled a large surrounding normal gland including the same image acquisition plane in the same depth and without obvious vessels. The patient was a 36-year-old man with PTMC (1.0 cm diameter) and *BRAF* mutation. Relative TTP was 1.05, the tumor was well defined, punctate echogenic foci were present, and the tumor was adjacent to the thyroid capsule. These data led to a score of 0.97 in the predictive model. ROI, regions of interest; TTP, time-to-peak; PTMC, papillary thyroid microcarcinoma.

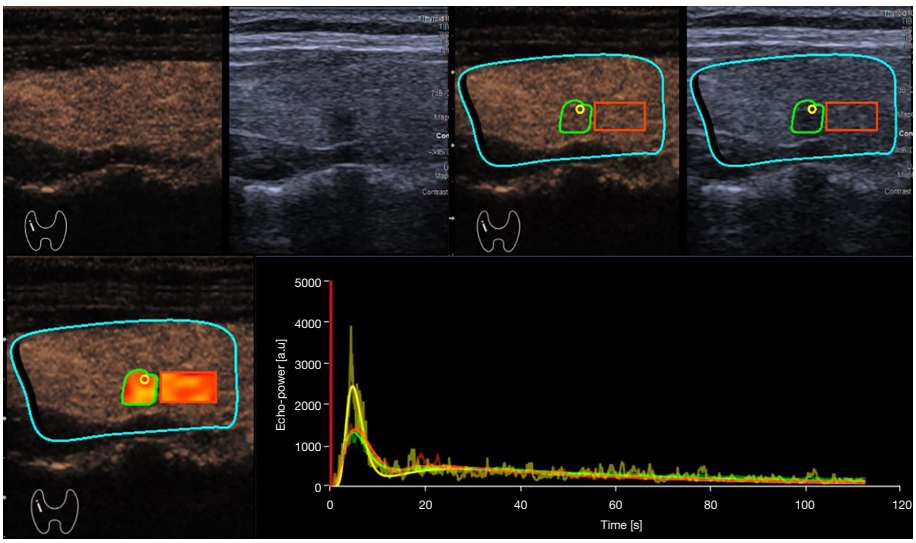

Figure 5 Another example of ultrasound analysis. Delimitation ROI (blue) delineates the processing area, excluding any non-echo data such as text, color bars, or image borders. ROI 1 (green) included the entire tumor boundary on conventional ultrasound with reference to the contrast-enhanced image. ROI 2 (yellow) included 1mm circles that targeted the greatest enhancement point, aided by the color-coded imaging and peak enhancement values generated by VueBox. ROI 3 (red) encircled a large surrounding normal gland including the same image acquisition plane in the same depth and without obvious vessels. The patient was a 32-year-old woman with PTMC (0.5 cm diameter) and wild-type *BRAF*. Relative TTP in the area of strongest enhancement was 0.92, the tumor border was ill defined, echogenic foci were absent, and the tumor was adjacent to thyroid capsules. These data led to a score of 0.57 in the predictive model. PTMC, papillary thyroid microcarcinoma; TTP, time to peak; ROI, region of interest.

Differences in qualitative data were assessed using the χ^2 test and Fisher's exact test. Statistical analyses were performed using SAS 9.4 (SAS Institute Inc., Cary, NC, USA). Results were expressed as mean ± standard deviation (SD) for quantitative variables, or as frequencies for categorical variables. P<0.05 was considered to indicate a statistically significant difference.

Independent ultrasound risk factors for BRAF mutation in PTMC were explored using multivariate stepwise logistic regression. Independent risk factors were used to develop a predictive model with the formula,

$$P = \frac{1}{1+e^{-(\alpha+\beta_1 x_1+\ldots+\beta_m x_m)}} \quad [1]$$

where P refers to the probability of *BRAF* mutation; α, intercept; and β, logistic regression coefficient. This model was assessed for accuracy using internal validation with a random seed number of 2021 in STATA 15 (StataCorp, College Station, TX, USA). Ten-fold cross-validation was performed, and bootstrapping was used to calculate the mean cross-validation area under the curve (cvAUC), along with the SD and 95% confidence interval (CI).

Results

Clinicodemographic characteristics of patients

A total of 103 patients (including 78 women), each with a single lesion, were enrolled in this study. Univariate analysis showed that tumors were significantly larger among patients with mutated *BRAF* (P=0.042), whereas the two groups of patients did not differ significantly in age or sex (*Table 1*).

Comparison of patient groups based on conventional ultrasonography

Patients with mutated or wild-type *BRAF* did not differ significantly in tumor location, shape, boundary, echogenicity, aspect ratio, or blood supply based on the color Doppler flow imaging (*Table 2*). The proportion of patients with echo heterogenicity was markedly higher among those with mutated BRAF than among those with wild-type *BRAF* (81.94% *vs.* 54.84%), as was the proportion of patients with echogenic foci (56.94% *vs.* 29.03%). Conversely, the proportion of patients with macrocalcifications was notably higher among patients with

Table 1 Demographic and clinicopathologic characteristics of 103 patients with papillary thyroid microcarcinoma, stratified by *BRAF* genotype

Characteristic	Mutant *BRAF* (n=72)	Wild-type *BRAF* (n=31)	P
Sex			0.445
Male	19 (26.39)	6 (19.35)	
Female	53 (73.61)	25 (80.65)	
Age, years			
Mean ± SD (range)	43.69±12.30 (26–78)	44.58±9.57 (32–66)	0.433*
<50	63 (70.79)	26 (72.22)	0.219**
≥50	26 (29.21)	10 (27.78)	
Tumor size (cm)			
Mean ± SD (range)	0.71±0.17 (0.30–1.00)	0.64±0.18 (0.35–1.00)	0.042*
≤0.5	13 (18.06)	13 (41.94)	0.010**
>0.5	59 (81.94)	18 (68.06)	
ACR TI-RADS score			
Mean ± SD (range)	9.46±1.87 (6–13)	10.03±1.68 (7–12)	0.133*
<7	5 (6.94)	0 (0.00)	
≥7	67 (83.06)	31 (1.00)	
Bethesda stage			0.001**
I	1 (1.39)	0 (0.00)	
III	2 (2.78)	1 (3.23)	
IV	1 (1.39)	0 (0.00)	
V	9 (12.50)	16 (51.61)	
VI	59 (81.94)	14 (45.16)	

Values are displayed as n (%), unless otherwise noted. *, Wilcoxon rank sum test; **, Chi-squared test. SD, standard deviation; ACR, American College of Radiology; TI-RADS, thyroid imaging, reporting and data system.

wild-type *BRAF* (6.94% *vs.* 12.90%), as was the proportion of patients with peripheral calcifications (2.78% *vs.* 3.23%).

Comparison of patient groups based on contrast-enhanced ultrasonography

Patients with mutated or wild-type *BRAF* did not differ significantly in enhancement degree, pattern, homogeneity, or completeness (*Table 3*). Similarly, they did not differ markedly in WiAUC, mTTl, WiR, WiPI, WoAUC, WiWoAUC, FT, or WoR. The relative rise time and relative TTP were considerably longer among patients with mutated *BRAF*. Also, the proportions of patients with relative TTP >1 in tumors and the strongest enhancement area within the tumor were significantly higher among those with mutated *BRAF*.

Independent ultrasound risk factors for mutated BRAF in PTMC

Several ultrasound findings emerged from the multivariate analysis as independent risk factors of *BRAF* mutation (*Table 4*): relative TTP for the area of strongest enhancement inside the tumor, unclear tumor boundary, tumor location adjacent to thyroid capsules, maximum tumor diameter >0.5 cm, and punctate echogenic foci. These factors were used to generate the following model to predict *BRAF* mutation (corresponding examples are shown in *Figures 4*,*5*):

P' = −1.799 + 1.761 (TTP of the strongest enhancement point >1) − 1.176 (blurred boundary) + 1.446 (adjacent to

Table 2 Comparison of conventional ultrasound features in 103 patients with papillary thyroid microcarcinoma, stratified by BRAF genotype

Feature	Mutant *BRAF* (n=72)	Wild-type *BRAF* (n=31)	P
Echogenicity			1.000
Hyperechoic or isoechoic	2 (2.78)	0 (0.00)	
Hypoechoic or very hypoechoic	70 (96.63)	31 (100.00)	
Echo homogeneity			0.004
Homogeneous	13 (18.06)	14 (45.16)	
Heterogeneous	59 (81.94)	17 (54.84)	
Echogenic foci			0.045
None	24 (33.33)	17 (54.84)	
Punctate echogenic foci	41 (56.94)	9 (29.03)	
Macrocalcifications	5 (6.94)	4 (12.90)	
Peripheral (rim) calcifications	2 (2.78)	1 (3.23)	
Location			0.118
Distal from capsules	17 (23.61)	12 (38.71)	
Adjacent to capsules	55 (76.39)	19 (61.29)	
Margin			0.430
Regular	7 (9.72)	1 (3.23)	
Irregular	65 (90.28)	30 (96.77)	
Boundary			0.064
Unclear	30 (41.67)	7 (22.58)	
Clear	42 (68.33)	24 (77.42)	
Aspect ratio			0.864
<1	22 (30.56)	10 (32.26)	
≥1	50 (69.44)	21 (67.74)	
Blood flow volume (Adler system*)			0.282
I	9 (10.11)	8 (22.22)	
II	14 (17.98)	7 (22.22)	
III	32 (41.57)	12 (41.67)	
IV	17 (30.34)	4 (13.89)	

Values are presented as n (%), unless noted otherwise. *, see Methods for description.

thyroid capsules) + 1.692 (maximum diameter >0.5 cm) + 1.226 (punctate echogenic foci) – 0.832 (peripheral/rim calcification) – 0.588 (macrocalcifications) (P'= logit P).

When we interpreted P>0.62 as indicative of the presence of *BRAF* mutation, the model showed moderate diagnostic performance: sensitivity, 77.8%; specificity, 64.5%; accuracy, 73.8%; Youden index, 0.432; and AUC, 0.824 (*Figure 6*). According to the Hosmer-Lemeshow χ^2 test, the model's goodness of fit was relatively high (P=0.54). Internal validation using 10-fold cross-validation showed a cvAUC of 0.723 (>0.7), with SD =0.170 and 95% CI: 0.591–0.814 (*Figure 7*), verifying moderate predictive value of the model.

Table 3 Comparison of the contrast-enhanced ultrasound features in 103 patients with papillary thyroid microcarcinoma, stratified by *BRAF* genotype

Feature	Mutant *BRAF* (n=72)	Wild-type *BRAF* (n=31)	P
Qualitative features			
Degree of enhancement			0.544
Hypoenhancement	53 (73.61)	21 (67.74)	
Isoenhancement or hyperenhancement	19 (26.39)	10 (32.26)	
Homogeneity of enhancement			0.276
Homogeneous	10 (13.89)	7 (22.58)	
Heterogeneous	62 (86.11)	24 (77.42)	
Completeness of enhancement			0.999
Incomplete	65 (90.28)	28 (90.32)	
Complete	7 (9.72)	3 (9.68)	
Pattern of enhancement			0.255
Centripetal	39 (54.17)	13 (41.94)	
Diffuse or centrifugal enhancement	33 (45.83)	18 (58.06)	
Quantitative CEUS			
Relative values for the whole tumor			
WiAUC 1	0.834 (0.618, 1.017)	0.872 (0.589, 0.973)	0.983
RT 1	1.064 (0.983, 1.156)	1.001 (0.934, 1.077)	0.019
mTTI 1	1.165 (0.952, 1.432)	1.038 (0.802, 1.271)	0.241
TTP 1	1.039 (1.003, 1.088)	0.982 (0.953, 1.027)	<0.001
WiR 1	0.713 (0.537, 0.890)	0.819 (0.499, 1.017)	0.206
WiPI 1	0.778 (0.578, 0.955)	0.842 (0.538, 1.032)	0.429
WoR 1	0.669 (0.479, 0.854)	0.770 (0.469, 1.051)	0.307
WoAUC 1	0.860 (0.634, 1.063)	0.937 (0.605, 1.181)	0.610
WiWoAUC 1	0.878 (0.642, 1.058)	0.916 (0.591, 1.102)	0.677
FT 1	1.102 (0.993, 1.240)	1.058 (0.924, 1.196)	0.235
Relative values for the area of strongest enhancement			
WiAUC 2	1.278 (0.926, 1.807)	1.203 (1.135, 1.615)	0.692
RT 2	0.987 (0.877, 1.091)	0.896 (0.762, 1.024)	0.063
mTTI 2	0.857 (0.518, 1.079)	0.799 (0.589, 1.070)	0.886
TTP 2	1.029 (0.950, 1.131)	0.978 (0.909, 1.060)	0.064
WiR 2	1.370 (0.946, 2.048)	1.590 (1.108, 2.081)	0.350
WiPI 2	1.401 (0.966, 1.866)	1.435 (1.065, 1.725)	0.555
WoR 2	1.445 (0.975, 2.025)	1.492 (1.215, 2.437)	0.307
WoAUC 2	1.274 (0.786, 1.853)	1.194 (0.893, 1.632)	0.880

Table 3 *(Continued)*

Table 3 *(Continued)*

Feature	Mutant *BRAF* (n=72)	Wild-type *BRAF* (n=31)	P
WiWoAUC 2	1.297 (0.843, 1.788)	1.184 (0.960, 1.626)	0.897
FT 2	0.960 (0.780, 1.115)	0.844 (0.672, 1.064)	0.152
Time-related relative variables			
RT 1			0.085
≤1	20 (27.78)	14 (45.16)	
>1	52 (72.22)	17 (54.84)	
RT 2			0.112
≤1	39 (54.17)	22 (70.97)	
>1	33 (45.83)	9 (29.03)	
mTTI 1			0.600
≤1	24 (33.33)	12 (38.71)	
>1	48 (66.67)	19 (61.29)	
mTTI 2			0.668
≤1	48 (66.67)	22 (70.97)	
1	24 (33.33)	9 (29.03)	
TTP 1			<0.001
≤1	17 (23.61)	21 (67.74)	
>1	55 (76.39)	10 (32.26)	
TTP 2			0.007
≤1	28 (38.89)	21 (67.74)	
>1	44 (61.11)	10 (32.26)	
FT 1			0.434
≤1	20 (27.78)	11 (35.48)	
>1	52 (72.22)	20 (64.52)	
FT 2			0.369
≤1	42 (58.33)	21 (67.74)	
>1	30 (41.67)	10 (32.26)	

Values are presented as n (%) or median (interquartile range), unless noted otherwise. CEUS, contrast-enhanced ultrasound; WiAUC, wash-in area under the curve; RT, rise time; mTTI, mean transit time local; TTP, time-to-peak; WiR, wash-in rate; WiPI, wash-in perfusion index; WoR, wash-out rate; WoAUC, wash-out area under the curve; WiWoAUC, wash-in and wash-out areas under the curve; FT, fall time.

Discussion

The rate of *BRAF* mutation among our PTMC patients was 70%, which was comparable to the rates in other Chinese, Japanese, and Caucasian patient populations (14,21-23). *BRAF* mutation leading to Val600Glu substitution in the protein strongly increases its activity, upregulates RAF/MEK (mitogen-activated protein kinase kinase) signaling (24,25), and stimulates cell division, proliferation, and

Table 4 Multivariate regression to identify the independent predictors of *BRAF* mutation in patients with papillary thyroid microcarcinoma

Potential predictor and categories	β	OR	95% CI	P
TTP 2b				
≤1 (reference)	0.000	1.000	–	–
>1	1.761	5.819	1.841–18.399	0.003
Boundary				
Unclear (reference)	0.000	1.000	–	–
Clear	–1.176	0.309	0.096–0.992	0.049
Echogenic foci				
None or large comet-tail artifacts (reference)	0.000	1.000	–	–
Punctate echogenic foci	1.226	3.408	1.108–10.481	0.032
Peripheral (rim) calcifications	–0.832	0.435	0.066–2.853	0.386
Macrocalcifications	–0.588	0.556	0.031–10.057	0.691
Location				
Distal from capsules (reference)	0.000	1.000	–	–
Adjacent to capsules	1.446	4.246	1.250–14.415	0.020
Size (cm)				
≤0.5 (reference)	0.000	1.000	–	–
>0.5	1.692	5.431	1.631–18.079	0.006
Intercept	–1.799	–	–	0.051

All variants that showed significance and selective variants that did not show significance in the univariate analysis were included in the multivariate analysis. OR, odds ratio; CI, confidence interval; TTP, time-to-peak.

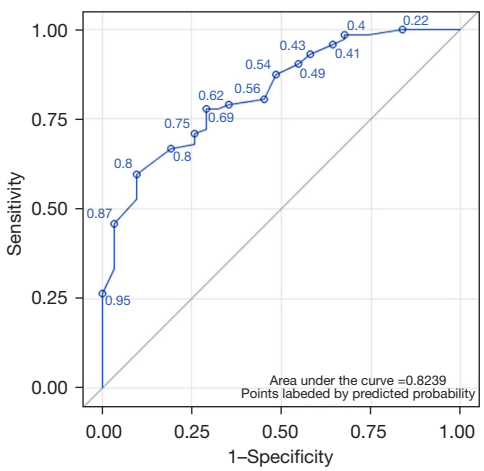

Figure 6 Receiver operating characteristic curve for multivariate stepwise regression. All of the statistically significant factors (P<0.05) and selective factors without statistical significance (P>0.05) in the univariate analysis were then used in the logistic analysis.

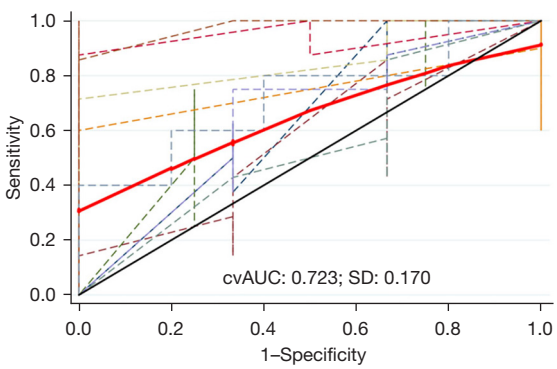

Figure 7 Ten-fold cross-validation of the model to predict BRAF mutation in patients with PTMC. The dashed lines depict the receiver operating characteristic curves, the solid red line represents the 10-fold mean cvAUC, and the solid black line denotes the reference line for perfect performance. The mean cvAUC was 0.723, with SD =0.170 and 95% CI: 0.591–0.814. cvAUC, cross-validation area under the curve; SD, standard deviation; PTMC, papillary thyroid microcarcinoma; CI, confidence interval.

differentiation in thyroid cancers (7,24,26). Herein, we showed evidence that combining conventional and contrast-enhanced ultrasonography may provide a relatively straightforward, non-invasive way to predict *BRAF* mutation in patients with PTMC, without the need for invasive FNAB. We developed a model to predict such mutation based on five ultrasound features: TTP in strongest enhancement, tumor boundary, presence of echogenic foci, tumor location, and maximum tumor diameter.

Of all the conventional ultrasound features that we assessed, only two were significantly associated with *BRAF* mutation: the presence of echo homogeneity and punctate echogenic foci. In contrast to another study of Asian patients, we did not observe a significant association with nodule margin (27). We observed that the presence of microcalcifications was associated with *BRAF* mutation, in contrast to some previous research (18), but similar to several other studies of Chinese and American patients (14,28,29). Yet, other studies have failed to detect significant associations between conventional ultrasound features and *BRAF* mutation (17,18,21). This discrepancy in the literature highlights the need for further investigation in this area, including external validation of our predictive model.

Moreover, of all the contrast-enhanced ultrasound features that we assessed, *BRAF* mutation was significantly associated with a longer rise time and TTP. This may indicate greater fibroblastic stromal response, resistance to apoptosis, cell proliferation, and angiogenesis (30), which leads to greater vascularization (15,31). Consistent with our findings, a study of another Chinese patient cohort showed that *BRAF* mutation was associated with TTP (16). We did not observe significant associations between *BRAF* mutation and centripetal, insignificant, or complete enhancement, in contrast to previous work (14,15). Our negative findings should be verified in larger samples, especially since differences in angiogenesis may be smaller in PTMC than in the larger tumors in several previous studies (14,15) and therefore require greater statistical power to detect.

Our results should be interpreted with caution considering that there were several limitations in this study. Firstly, the retrospective design and relatively small sample of patients, all of whom had been definitively diagnosed with PTMC based on fine-needle aspiration biopsy. Also, since PTMCs cannot represent all high-risk nodules, the predictive model described here must be validated using patient populations with high-risk sonographic features, including hypoechoic, aspect ratio ≥1, irregular margin, and echogenic foci. Another limitation is that a single researcher conducted all of the quantitative analyses, preventing us from assessing the effects of inter-observer variability that is inevitable in the clinic. Similarly, our analyses reflect only a few clinicians' interpretations of ultrasound images, which can differ from center to center. Thirdly, the pathological subtype analyses were more accurately conducted with surgical resection samples rather than with tissues obtained by fine-needle aspiration, so we cannot exclude that our results may have been affected by different subtypes of PTMC. Furthermore, limited sample size enabled internal validation, which is inferior to external validation. Given these limitations, our findings should be verified and extended in larger studies, preferably with a prospective, multicenter design.

Acknowledgments

Funding: The study was supported by National Natural Science Foundation of China (No. 81971627), and China Japan Friendship Hospital talent introduction project (No. 2019-RC-2).

Footnote

Reporting Checklist: The authors have completed the STARD reporting checklist. Available at https://gs.amegroups.com/article/view/10.21037/gs-22-493/rc

Data Sharing Statement: Available at https://gs.amegroups.com/article/view/10.21037/gs-22-493/dss

Conflicts of Interest: All authors have completed the ICMJE uniform disclosure form (available at https://gs.amegroups.com/article/view/10.21037/gs-22-493/coif). All authors report that the study was supported by National Natural Science Foundation of China (No. 81971627), and China Japan Friendship Hospital talent introduction project (No. 2019-RC-2). SL is from Bracco Imaging Medical Technologies Co., Ltd. The other authors have no conflicts of interest to declare.

Ethical Statement: The authors are accountable for all aspects of the work in ensuring that questions related to the accuracy or integrity of any part of the work are appropriately investigated and resolved. The study was conducted in accordance with the Declaration of Helsinki (as revised in 2013). The study was approved by institutional

ethics board of China-Japan Friendship Hospital (No. 2019-103-K71). Individual consent for this retrospective analysis was waived.

References

1. Du L, Li R, Ge M, et al. Incidence and mortality of thyroid cancer in China, 2008-2012. Chin J Cancer Res 2019;31:144-51.
2. Haugen BR, Alexander EK, Bible KC, et al. 2015 American Thyroid Association Management Guidelines for Adult Patients with Thyroid Nodules and Differentiated Thyroid Cancer: The American Thyroid Association Guidelines Task Force on Thyroid Nodules and Differentiated Thyroid Cancer. Thyroid 2016;26:1-133.
3. Rossi ED, Pantanowitz L, Hornick JL. A worldwide journey of thyroid cancer incidence centred on tumour histology. Lancet Diabetes Endocrinol 2021;9:193-4.
4. Li F, Chen G, Sheng C, et al. BRAFV600E mutation in papillary thyroid microcarcinoma: a meta-analysis. Endocr Relat Cancer 2015;22:159-68.
5. Xu X, Quiros RM, Gattuso P, et al. High prevalence of BRAF gene mutation in papillary thyroid carcinomas and thyroid tumor cell lines. Cancer Res 2003;63:4561-7.
6. Shaha AR, Tuttle RM. Thyroid cancer staging and genomics. Ann Transl Med 2019;7:S49.
7. Fallahi P, Ferrari SM, Galdiero MR, et al. Molecular targets of tyrosine kinase inhibitors in thyroid cancer. Semin Cancer Biol 2022;79:180-96.
8. Xing M, Haugen BR, Schlumberger M. Progress in molecular-based management of differentiated thyroid cancer. Lancet 2013;381:1058-69.
9. Xing M, Alzahrani AS, Carson KA, et al. Association between BRAF V600E mutation and recurrence of papillary thyroid cancer. J Clin Oncol 2015;33:42-50.
10. Huang Y, Qu S, Zhu G, et al. BRAF V600E Mutation-Assisted Risk Stratification of Solitary Intrathyroidal Papillary Thyroid Cancer for Precision Treatment. J Natl Cancer Inst 2018;110:362-70.
11. Kim KJ, Kim SG, Tan J, et al. BRAF V600E status may facilitate decision-making on active surveillance of low-risk papillary thyroid microcarcinoma. Eur J Cancer 2020;124:161-9.
12. Silver JA, Bogatchenko M, Pusztaszeri M, et al. BRAF V600E mutation is associated with aggressive features in papillary thyroid carcinomas ≤ 1.5 cm. J Otolaryngol Head Neck Surg 2021;50:63.
13. Ulisse S, Baldini E, Lauro A, et al. Papillary Thyroid Cancer Prognosis: An Evolving Field. Cancers (Basel) 2021;13:5567.
14. Liu Y, He L, Yin G, et al. Association analysis and the clinical significance of BRAF gene mutations and ultrasound features in papillary thyroid carcinoma. Oncol Lett 2019;18:2995-3002.
15. Lin ZM, Yan CX, Song Y, et al. The features of contrast enhanced ultrasound and BRAF V600E in papillary thyroid carcinoma. J Thorac Dis 2019;11:5071-8.
16. Chen L, Chen L, Liu J, et al. The Association Among Quantitative Contrast-Enhanced Ultrasonography Features, Thyroid Imaging Reporting and Data System and BRAF V600E Mutation Status in Patients With Papillary Thyroid Microcarcinoma. Ultrasound Q 2019;35:228-32.
17. Li Q, Yuan J, Wang Y, et al. Association between the BRAF V600E mutation and ultrasound features of the thyroid in thyroid papillary carcinoma. Oncol Lett 2017;14:1439-44.
18. Hwang J, Shin JH, Han BK, et al. Papillary thyroid carcinoma with BRAFV600E mutation: sonographic prediction. AJR Am J Roentgenol 2010;194:W425-30.
19. Fu Y, Feng Q, Zhang S, et al. Application of oxytocin in ultrasound-guided percutaneous microwave ablation for treatment of hypervascular uterine fibroids: a preliminary report. Int J Hyperthermia 2019;36:761-7.
20. Dietrich CF, Averkiou MA, Correas JM, et al. An EFSUMB introduction into Dynamic Contrast-Enhanced Ultrasound (DCE-US) for quantification of tumour perfusion. Ultraschall Med 2012;33:344-51.
21. Kwak JY, Kim EK, Chung WY, et al. Association of BRAFV600E mutation with poor clinical prognostic factors and US features in Korean patients with papillary thyroid microcarcinoma. Radiology 2009;253:854-60.
22. Melck AL, Yip L, Carty SE. The utility of BRAF testing in the management of papillary thyroid cancer. Oncologist 2010;15:1285-93.
23. Lee JH, Lee ES, Kim YS. Clinicopathologic significance

of BRAF V600E mutation in papillary carcinomas of the thyroid: a meta-analysis. Cancer 2007;110:38-46.
24. Young A, Lyons J, Miller AL, et al. Ras signaling and therapies. Adv Cancer Res 2009;102:1-17.
25. Romei C, Elisei R. A Narrative Review of Genetic Alterations in Primary Thyroid Epithelial Cancer. Int J Mol Sci 2021;22:1726.
26. Perri F, Pezzullo L, Chiofalo MG, et al. Targeted therapy: a new hope for thyroid carcinomas. Crit Rev Oncol Hematol 2015;94:55-63.
27. Shangguan R, Hu YP, Huang J, et al. Association Between BRAFV600E Mutation and the American College of Radiology Thyroid Imaging, Reporting and Data System in Solitary Papillary Thyroid Carcinoma. Acad Radiol 2019;26:154-60.
28. Khadra H, Deniwar A, Mohsin K, et al. Can Suspicious Ultrasound Features Predict BRAFV600E Status in Papillary Thyroid Cancer? Eur Thyroid J 2018;7:205-10.
29. Kabaker AS, Tublin ME, Nikiforov YE, et al. Suspicious ultrasound characteristics predict BRAF V600E-positive papillary thyroid carcinoma. Thyroid 2012;22:585-9.
30. Xing M, Usadel H, Cohen Y, et al. Methylation of the thyroid-stimulating hormone receptor gene in epithelial thyroid tumors: a marker of malignancy and a cause of gene silencing. Cancer Res 2003;63:2316-21.
31. Li R, Hao J, Zhu Z, et al. Correlation between US-FNAC with BRAF V600E Mutation Analysis and Central Neck Lymph Node Metastasis in cN0 Papillary Thyroid Cancer. Biomed Res Int 2021;2021:9937742.

(English Language Editor: A. Kassem)

Cite this article as: Li H, Ma J, Xi X, Tang J, Wang L, Wang L, Lin S, Zhang B. The analysis and validation of the prediction value of conventional and contrast-enhanced ultrasonography for *BRAF* mutant papillary thyroid microcarcinoma. Gland Surg 2022;11(10):1683-1696. doi: 10.21037/gs-22-493